A tetrairon(III) single-molecule magnet and its solvatomorphs: synthesis, crystal structures and vapor-phase processing

Andrea Cornia [a,*], Andrea Nava [a,b], Valeria Lanzilotto [c,1], Giordano Poneti [d], Matteo Mannini [c], Roberta Sessoli [c]

[a] *Department of Chemical and Geological Sciences and INSTM Research Unit, University of Modena and Reggio Emilia, Via G. Campi 103, 41125 Modena, Italy*
[b] *Department of Physics, Informatics and Mathematics, University of Modena and Reggio Emilia, Via G. Campi 213/a, 41125 Modena, Italy*
[c] *Department of Chemistry "U. Schiff" and INSTM Research Unit, University of Florence, Via della Lastruccia 3-13, 50019 Sesto Fiorentino (FI), Italy*
[d] *Instituto de Química, Universidade Federal do Rio de Janeiro, Avenida Athos da Silveira Ramos 149, Centro de Tecnologia – Cidade Universitária, 21941-909 Rio de Janeiro, Brazil*

A B S T R A C T

With the aim of investigating the impact of lattice solvent on the processability of tetrairon(III) single-molecule magnets by thermal sublimation, two new solvatomorphs of $[Fe_4(L^{Ph})_2(dpm)_6]$ (**1**) were prepared and structurally characterized along with unsolvated **1** (H_3L^{Ph} = 2-(hydroxymethyl)-2-phenylpropane-1,3-diol, Hdpm = dipivaloylmethane). All solvatomorphs crystallize in the $C2/c$ space group whereas solvent-free **1** belongs to a different space group ($P2_1/c$). The pitch of the propeller-like tetrairon(III) molecules is distinctly different in solvated vs. unsolvated phases, highlighting the effect of intermolecular interactions and crystal packing. The compounds sublime at 450–490 K (in high vacuum conditions, $\sim10^{-6}$–10^{-7} mbar) affording thick deposits which display different crystallinity depending on the particular starting material used. However, all sublimed samples retain slow magnetic relaxation with thermal activation parameters comparable to those of microcrystalline **1**. The results indicate that factors other than mere molecular structure have a limited influence on the processability of these materials by thermal sublimation.

1. Introduction

The processing of single-molecule magnets (SMMs) into films with variable thickness, down to monolayers or submonolayers [1,2], is motivated by the perspective use of these magnetically bistable materials in spintronic devices [3] or as individually addressable, surface-supported magnetic bits [4]. A major breakthrough in the field was the recent discovery that some organometallic monodysprosium(III) SMMs retain a memory effect above the normal boiling point of liquid dinitrogen [5–7]. The real application potential [8] of most SMMs, however, is severely limited by their instability under the processing methods customarily used in spintronics, above all thermal sublimation in high vacuum (HV). Some mononuclear SMMs withstand sublimation, like those of the $LnPc_2$ [9–14] and Ln(trensal) [15–17] families, as well as a few other lanthanoid (Ln) complexes [18–20] (H_2Pc = phthalocyanine, $H_3trensal$ = 2,2′,2″-tris(salicylideneimino)triethylamine). Polynuclear SMMs suitable for vapor phase processing are also known and

include triple-decker Ln_2Pc_3 derivatives [9,11,21], a Dy_2 species [22,23], and endohedral fullerenes [24].

Some tetrairon(III) compounds with formula $[Fe_4(L^R)_2(dpm)_6]\cdot$solv are also sublimable (Hdpm = dipivaloylmethane, solv = lattice solvent). This family of SMMs have a propeller-like structure enveloped by a bulky shell of twelve tBu groups and held together by two tripodal $(L^R)^{3-}$ ligands (H_3L^R = 2-R-2-(hydroxymethyl)propane-1,3-diol). A number of derivatives have been prepared and characterized which differ in the R substituent and/or in the presence and nature of lattice solvent [25]. The phenyl derivative (**1**, R = Ph), for instance, is best isolated as the diethyl ether solvate $\mathbf{1}\cdot Et_2O$ [26]. This compound was sublimed at 500±10 K in HV (10^{-7} mbar) to give $\sim$100 nm thick deposits which showed slow magnetic relaxation similar to the pristine material [27]. The same processing technique operated in ultra-HV was used with success to prepare monolayers and submonolayers of **1** on Au(111) [28,29], Cu(100) [29], and Cu_2N/Cu(100) [29,30] surfaces. These studies indicated that structurally and functionally intact Fe_4 complexes can be

---

transferred onto the surface, as proved by on-surface magnetometry [28], although smaller fragments are often co-deposited [29]. Fluorinated variants of **1** [31,32] and the derivative with R = CH_2SCH_3 (**2**), isolated as **2**·0.5Et_2O [33], are also sublimable.

In an attempt to clarify whether factors other than mere molecular structure influence processability, we have prepared two new solvatomorphs of **1**, namely **1**·C_7H_8 and **1**·2CCl_4, which are isostructural with previously reported **1**·Et_2O [26] and **1**·C_6H_6 [34]. In the course of this study, we were also able to isolate solvent-free **1**, which however crystallizes in a different space group than do solvated phases. We found that all these compounds with R = Ph show similar sublimation temperatures in HV and afford deposits with different crystallinity depending on the used pristine material. However, all sublimed samples retain slow magnetic relaxation with thermal activation parameters similar to microcrystalline **1**.

2. Experimental

General procedures. All synthetic operations were conducted with exclusion of moisture using reagent grade solvents, unless otherwise stated. Methanol was carefully dried over $Mg(OMe)_2$ and distilled prior to use [35,36], while pentachloroethane was purified and distilled as described in Ref. [35]. Compounds **1**·Et_2O and **1**·C_6H_6 were prepared as previously reported [26,34]. Microanalytical CHN determinations were carried out on microcrystalline samples of all compounds using a Carlo Erba EA1110 CHNS-O automatic analyzer.

Synthesis of [Fe$_4$(L^{Ph})$_2$(dpm)$_6$]·C$_7$H$_8$ (1·C$_7$H$_8$): **1**·Et_2O (0.037 g, 0.021 mmol) was dissolved in 0.5 mL of toluene. Slow evaporation over vaseline oil (4 mL) overnight under reduced pressure (440 torr) gave orange-red crystals (0.029 g, 78% yield). Anal. Calcd (%) for $C_{93}H_{144}Fe_4O_{18}$ (1773.51): C, 62.98; H, 8.18. Found: C, 62.61; H, 8.10.

Synthesis of [Fe$_4$(L^{Ph})$_2$(dpm)$_6$]·2CCl$_4$ (1·2CCl$_4$): **1**·Et_2O (0.027 g, 0.015 mmol) was dissolved in 0.5 mL of tetrachloromethane. Slow vapor diffusion of methanol (5 mL) gave orange-red crystals after three days (0.026 g, 85% yield). Anal. Calcd (%) for $C_{88}H_{136}Cl_8Fe_4O_{18}$ (1989.01): C, 53.14; H, 6.89. Found: C, 52.96; H, 6.62.

Synthesis of [Fe$_4$(L^{Ph})$_2$(dpm)$_6$] (1): **1**·Et_2O (0.056 g, 0.032 mmol) was dissolved in 2 mL of pentachloroethane. Slow evaporation over vaseline oil (10 mL) over two weeks under reduced pressure (260 torr) gave orange-red crystals (0.044 g, 82% yield). Anal. Calcd (%) for $C_{86}H_{136}Fe_4O_{18}$ (1681.37): C, 61.43; H, 8.15. Found: C, 61.32; H, 8.20.

X-ray Crystallography. Single-crystal X-ray structure determinations on **1**·C_7H_8 and **1**·2CCl_4 were carried out at 140(2) K on a Bruker-Nonius X8APEX diffractometer equipped with Mo-Kα generator, area detector, and Kryoflex liquid dinitrogen cryostat. Measurements on **1** were conducted on the same instrument at 150(2) and 298(2) K. The structures were solved and refined on F_o^2 by standard methods, using SIR92 [37] and SHELXL-97, SHELXL-2014/7 or SHELXL-2018/3 [38] software, and the WINGX suite [39]. All nonhydrogen atoms were refined anisotropically, unless otherwise noted, while H atoms were added in idealized positions, allowed to ride on the parent C atoms and treated isotropically with $U(H) = 1.5U_{eq}(C)$ for methyl hydrogens and $U(H) = 1.2U_{eq}(C)$ for the remaining H atoms. When deemed necessary, anisotropic displacement parameters (ADPs) were subject to rigid body (DELU) and/or quasi-isotropy (ISOR) restraints.

In **1**·C_7H_8, one tBu group shows rotational disorder over two positions with 0.580(8):0.420(8) occupancies. The two components were forced to have a similar geometry (SAME) and their quaternary C atoms were assigned the same ADPs. Toluene molecule is disordered around a twofold axis and was refined with 0.5 occupancy and a unique isotropic displacement parameter (IDP) for its C atoms. The C skeleton was restrained to have mmm symmetry, with a regular hexagonal geometry (C–C = 1.39 Å) for the phenyl ring (AFIX 66) and a C–CH$_3$ distance of 1.51(1) Å (DFIX).

In **1**·2CCl_4, two tBu groups show rotational disorder over three and two positions, respectively, with 0.551(3):0.197(3):0.252(3) and 0.753(6):0.247(6) occupancies, respectively. Minority tBu groups were forced to have a similar geometry to a reference, non disordered $tert$-butyl in the structure (SAME). Their quaternary C atoms were constrained to have the same ADPs as those of the corresponding majority component, and a common IDP was assigned to their methyl carbons. Restraints (SADI) were also applied to the C(O)–C(CH$_3$)$_3$ distances involving disordered tBu groups. Three positions were resolved for the disordered CCl_4 molecule, with refined occupancies 0.734(2):0.131(2):0.135(2), constrained to sum up to unity. The minority components were forced to have a similar geometry (SAME) to the majority one and were treated isotropically, with one common displacement parameter for Cl and one for C atoms. The latter was restrained to be similar to that of the majority component (SIMU).

In the structure of **1** at 150(2) K one tBu group shows rotational disorder over two positions with 0.846(5):0.154(5) occupancies. The two components were restrained to have a similar geometry (SAME) and quaternary C atoms with the same ADPs. A common IDP was assigned to the methyl carbons of the minority component. The room-temperature structure of **1**, determined on the same crystal, showed very elongated ADPs for the methyl carbons of most tBu groups and converged to higher R-indices. A few C–CH$_3$ distances within tBu groups were restrained to 1.51(1) Å (DFIX). Crystal data and refinement parameters for the three low-temperature structures described in this paper are given in Table S1. Graphics utilized ORTEP-3 for Windows v2014.1 [39] and POV-Ray for Windows v3.7 [40]. CCDC 2113116–2113119 contain the supplementary crystallographic data for this paper. These data can be obtained free of charge from The Cambridge Crystallographic Data Centre via www.ccdc.cam.ac.uk/data_request/cif.

Thermal sublimation. Thermal sublimation of **1**·C_7H_8, **1**·2CCl_4, **1**·C_6H_6, and unsolvated **1** was performed in HV conditions ($P_{base} = 10^{-6}$–10^{-7} mbar) from a quartz crucible resistively heated up to the sublimation temperature of 450–490 K (temperature was monitored by a K-type thermocouple inserted into the crucible). Film growth was performed on a support (mica disk) covered with a Teflon® tape by keeping the powders at the sublimation temperature for ca. 2 days (**1**·C_7H_8), 4 days (**1**·2CCl_4), 18 h (**1**·C_6H_6), and 27 h (**1**). The mass of the deposits was 1.52 mg (**1**·C_7H_8), 1.46 mg (**1**·2CCl_4), 0.74 mg (**1**·C_6H_6), and 0.90 mg (**1**), and was measured by difference ($W_{(Teflon® + deposit)} - W_{Teflon®}$). As for the film thickness, the deposition rate was checked before and after deposition by a quartz crystal microbalance (QCM). However, after long-lasting processing the deposition rate usually depletes and the QCM-based thickness evaluation was only possible for **1**·C_6H_6 (ca. 500 nm). By using the mass and thickness values of **1**·C_6H_6, we estimated a thickness of about 600 nm for **1** and ca. 1000 nm for **1**·2CCl_4 and **1**·C_7H_8.

X-ray Powder Diffraction. X-Ray powder diffraction data were acquired on the sublimed samples using a Bruker New D8 Advance DAVINCI diffractometer in a theta-theta configuration equipped with a linear detector. The scans were collected in the 5–20° range of 2θ with Cu-Kα radiation (λ = 1.540 Å). Powder patterns were simulated with Mercury 2021.1.0 [41] using a full-width-at-half-maximum of 0.1° in 2θ.

Magnetic measurements. Alternating current (AC) magnetic investigations in the frequency range ν = 10–1000 Hz were performed on a Quantum Design MPMS instrument, using an oscillating field amplitude of 1–3 Oe and working in both zero and 1 kOe applied static fields (H_{DC}). Measurements were carried out on a grinded and pelletized microcrystalline sample of **1** wrapped in Teflon® tape, and on sublimed deposits prepared from **1**·C_7H_8, **1**·2CCl_4, **1**·C_6H_6, and unsolvated **1**, collected on Teflon® tape. In-phase and out-of-phase molar susceptibilities (hereafter indicated as χ_M' and χ_M'', respectively) were calculated using a molar mass of 1681.35 g/mol, as appropriate for unsolvated **1**. The data

were analyzed within the extended Debye model [42], in which a maximum in χ_M'' is observed when the relaxation time τ equals $\omega^{-1} = (2\pi\nu)^{-1}$ and allowance is made for a distribution of relaxation times described by parameter α. The value of τ at each temperature was determined by fitting the frequency dependence of χ_M'' to equation (1):

$$\chi_M''(\omega) = (\chi_T - \chi_S)\frac{(\omega\tau)^{1-\alpha}\cos\frac{\pi\alpha}{2}}{1 + 2(\omega\tau)^{1-\alpha}\sin\frac{\pi\alpha}{2} + (\omega\tau)^{2-2\alpha}} \quad (1)$$

where χ_T and χ_S are the isothermal and adiabatic molar susceptibilities, i.e. the molar susceptibilities observed in the two limiting cases $\nu \to 0$ and $\nu \to \infty$, respectively. The individual values of χ_T and χ_S, as well as a more reliable value of α, were evaluated by fitting isothermal $\chi_M''(\chi_M')$ data (Cole-Cole plot) [42] to equation (2):

$$\chi_M''(\chi_M') = -\frac{\chi_T - \chi_S}{2}\tan\frac{\pi\alpha}{2}$$
$$+ \left[\left(\frac{\chi_T - \chi_S}{2}\tan\frac{\pi\alpha}{2}\right)^2 + (\chi_M' - \chi_S)(\chi_T - \chi_M')\right]^{1/2} \quad (2)$$

The temperature dependence of the relaxation time was then fitted to Arrhenius equation (3):

$$\tau(T) = \tau_0\exp[\Delta/(k_BT)] \quad (3)$$

where Δ is the effective energy barrier to magnetic moment reversal, τ_0 is a pre-exponential factor and k_B is the Boltzmann constant.

3. Results and discussion

Synthesis and X-ray structures. Crystalline solvates of **1** with toluene (**1**·C$_7$H$_8$), tetrachloromethane (**1**·2CCl$_4$), and benzene (**1**·C$_6$H$_6$) [34] were obtained by recrystallizing **1**·Et$_2$O [26] from appropriate solvents. The unsolvated form **1** was first obtained as a byproduct of the synthesis of **1**·Et$_2$O, when the methanol-rich mother solution recovered after isolation of the compound was subject to further diffusion of methanol vapors for several weeks. These solvent-free crystals were then deliberately prepared by recrystallizing **1**·Et$_2$O from freshly-distilled pentachloroethane, a bulkier solvent.
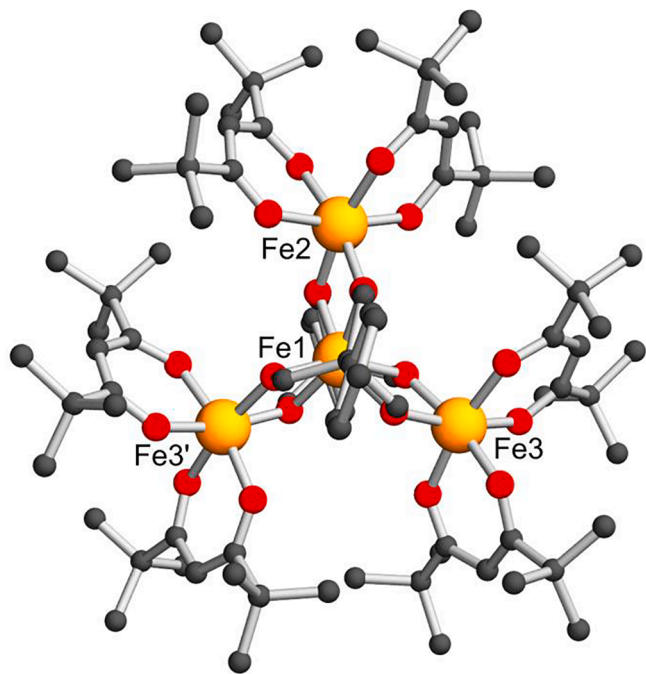

Fig. 1. Molecular structure of **1** in **1**·C$_7$H$_8$, viewed approximately normal to the molecular plane. Color code: orange = Fe, red = O, grey = C. The lattice toluene molecule, disorder effects, and H atoms are omitted for clarity.

The X-ray structure of **1** in **1**·C$_7$H$_8$ is displayed in Fig. 1 as an example. The four metals exhibit a metal-centered triangular arrangement, with the two tripodal (L^{Ph})$^{3-}$ ligands bridging the central (Fe1) and peripheral (Fe2, Fe3, Fe3′) metals, and the six dpm$^-$ anions providing terminal ligation to Fe2, Fe3 and Fe3′. **1**·C$_7$H$_8$ and all known solvated phases of **1** belong to monoclinic space group $C2/c$ and their crystal structure entails four tetrairon(III) molecules per unit cell. The asymmetric unit includes half a tetrairon(III) complex, with two iron(III) ions (Fe1 and Fe2) located on a twofold axis. Consequently, the Fe$_4$ molecules have crystallographically imposed twofold symmetry and the four metal centers are exactly coplanar. Selected geometrical parameters are gathered in Table 1 together with those of **1**·Et$_2$O [26] and **1**·C$_6$H$_6$ [34] for comparison (a more complete listing is available in Table S2). Within the series of solvated phases, molecular geometry undergoes only minor variations as a function of lattice solvent. An especially important geometrical parameter is the inclination (γ_{cp}) of each Fe$_c$(O)$_2$Fe$_p$ (mean) plane with respect to the (mean) plane through the four metals (here Fe$_c$ and Fe$_p$ denote the central and peripheral metals, respectively). The average value of γ_{cp} in a molecule is referred to as the "helical pitch" (γ) of the propeller-like structure. In the four solvates of **1**, the inclination values are remarkably similar within each compound and in different solvatomorphs (68.5–68.8°). The trigonal distortion parameters θ and ϕ for Fe$_c$ are also very close [25,43,44].

Of course, because of the centrosymmetric space group, the crystals are racemic mixtures of right- and left-handed propellers. Solvent molecules reside in four symmetry-equivalent cavities per unit cell, located around twofold axes and showing individual volumes of 290, 345, 270, and 302 Å^3 in the structures of **1**·C$_7$H$_8$, **1**·2CCl$_4$, **1**·Et$_2$O [26], and **1**·C$_6$H$_6$ [34], respectively.

Crystals of unsolvated **1** belong to centrosymmetric monoclinic space group $P2_1/c$; in this case, eight tetrairon(III) molecules are present in the unit cell. The asymmetric unit in fact contains two crystallographically independent Fe$_4$ complexes (mol A: Fe1–Fe4; mol B: Fe5–Fe8) which differ in the conformation of tBu and Ph substituents (Fig. 2). The four Fe atoms in each molecule lie on the same plane within 0.0011 (mol A) and 0.0030 Å (mol B), and the two molecules are almost coplanar (the average planes through the metals form a dihedral angle of 8.91(1)°). As shown in Table 1 and S2, mol A and mol B have very similar metrical parameters, with γ_{cp} varying from 69.3 to 70.6° in mol A and from 69.4 to 70.7° in mol B, and a virtually identical γ (70.1 and 70.0°, respectively). Notably, the helical pitch is distinctly larger than in the solvate series (68.6–68.8°). Because of the correlation between γ and ϕ [43], the distortion of the coordination sphere of Fe$_c$ by trigonal rotation is also approximately 2° larger than in the solvated phases ($\phi = 30.5$–30.8° vs 32.5–32.8°). Since the tetrairon(III) molecule remains exactly the same, the observed differences prove that intermolecular interactions and crystal-packing effects play an important role in determining molecular geometry [43]. The unit cell of **1** contains 4.7% of solvent-accessible voids, which individually do not exceed 83 Å^3 and are thus unsuitable to host pentachloroethane molecules.

Structure and magnetization dynamics of sublimed samples. Samples of **1**·C$_7$H$_8$, **1**·2CCl$_4$, **1**·C$_6$H$_6$, and unsolvated **1** were subject to thermal sublimation in HV at 450–490 K for a time sufficient to collect 1–2 mg of sublimed material on Teflon® tape. X-ray powder diffraction was used to get insight into the structure of these films. The low-angle ($2\theta = 5.5$–20°) diffraction patterns are presented in Fig. 3. Apart from the signals of Teflon® at 16.37 and 18.20°, the sample prepared from unsolvated **1** gives only two very weak diffraction peaks between 9 and 10° and is thus predominantly amorphous. The deposits obtained from the three solvatomorphs **1**·C$_7$H$_8$, **1**·2CCl$_4$, and **1**·C$_6$H$_6$ feature dominant diffraction peaks at 6.78(3) and 9.51(2)°, which highlight structural similarities between the samples. However, a set of weaker signals is also observed, which differ from sample to sample. For the sample obtained by sublimation of **1**·C$_7$H$_8$, the diffraction pattern agrees closely with the simulated pattern based on the structure of unsolvated **1** at room temperature (Fig. 3). However, sublimation of the tetrachloromethane and

Table 1
Selected geometrical parameters in compounds $1 \cdot C_7H_8$ (at 140 K), $1 \cdot 2CCl_4$ (at 140 K), $1 \cdot Et_2O$ (at 203 K), $1 \cdot C_6H_6$ (at 120 K), and 1 (at 150 K).

		$1 \cdot C_7H_8$	$1 \cdot 2CCl_4$	$1 \cdot Et_2O$ [a]	$1 \cdot C_6H_6$ [b]
Fe1···Fe2 (Å)		3.0797(6)	3.0824(6)	3.0780(8)	3.0789(8)
Fe1···Fe3 (Å)		3.0783(4)	3.0780(4)	3.0726(6)	3.0764(5)
θ (°) [c]		54.21	54.19	54.20	54.18
ϕ (°) [c]		32.76	32.74	32.51	32.62
γ_{cp} (°)	Fe1(O)$_2$Fe2	68.51(5)	68.72(6)	68.79(7)	68.77(8)
	Fe1(O)$_2$Fe3	68.69(4)	68.64(5)	68.77(6)	68.71(6)
γ (°) [d]		68.63	68.67	68.78	68.73

	1, mol A			1, mol B		
Fe$_c$···Fe$_p$ (Å)	Fe1···Fe2	Fe1···Fe3	Fe1···Fe4	Fe5···Fe6	Fe5···Fe7	Fe5···Fe8
	3.0736(4)	3.0917(4)	3.0857(4)	3.0776(5)	3.0833(5)	3.0848(4)
θ (°) [c]	53.95			53.91		
ϕ (°) [c]	30.51			30.79		
γ_{cp} (°)	Fe1(O)$_2$Fe2	Fe1(O)$_2$Fe3	Fe1(O)$_2$Fe4	Fe5(O)$_2$Fe6	Fe5(O)$_2$Fe7	Fe5(O)$_2$Fe8
	70.61(4)	69.33(4)	70.41(4)	70.73(4)	69.86(4)	69.37(4)
γ (°) [d]	70.12			69.99		

[a] Data taken from Ref. [26]. [b] Data taken from Ref. [34]. [c] The angles θ and ϕ describe the distortion of the coordination sphere of Fe$_c$ (averaged to D_3 symmetry) by trigonal compression/elongation and trigonal rotation, respectively. The extent of distortion is measured by the deviation of these angles from octahedral values (54.74 and 60°, respectively). [d] Average value of γ_{cp}. For details, see Refs. [25,43,44].
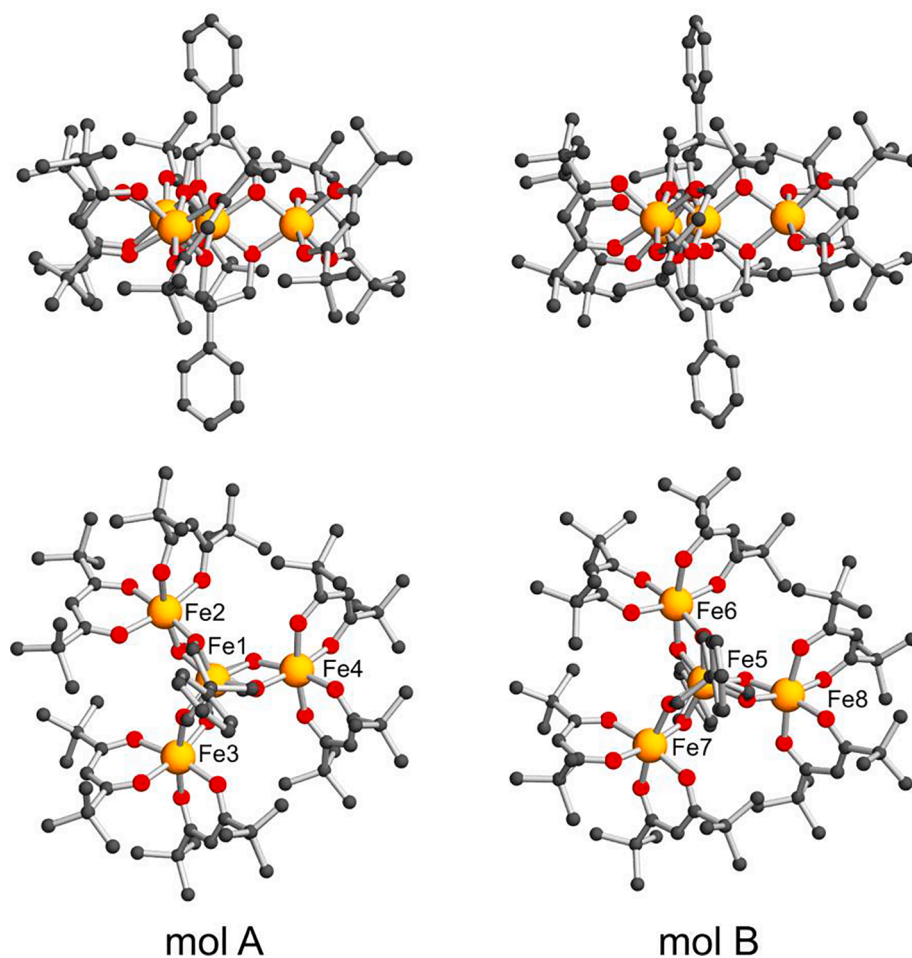

Fig. 2. Side (upper figures) and top (lower figures) views of the two crystallographically independent molecules in 1: mol A (left) and mol B (right). Color code is the same as in Fig. 1. Disorder effects and H atoms are omitted for clarity.

benzene solvates yields patterns which differ from that of the structurally characterized unsolvated phase. We have at present no definite explanation for such erratic behavior.

The dynamics of the magnetization of the deposits was investigated using frequency- and temperature-dependent AC susceptibility measurements. The same technique was used to characterize microcrystalline 1. With no static field applied, sublimed 1 displays a frequency dependent, non-zero χ_M'' but no peaks appear within our experimental frequency window (Fig. S1). Upon application of a 1 kOe static field, relaxation slows down and a set of frequency and temperature dependent peaks become clearly visible (Fig. S2), indicating a thermally activated reversal of the magnetic moment. Sublimed
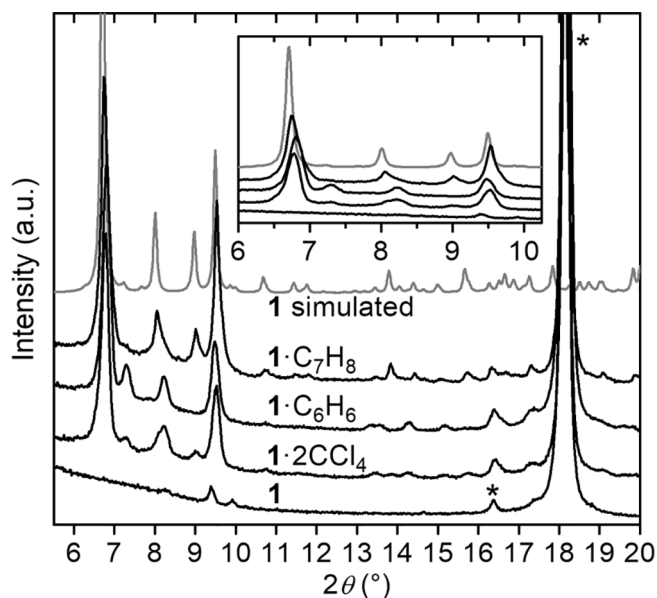
Fig. 3. Room-temperature powder diffractograms of sublimed films (black). Peaks marked with an asterisk are due to Teflon®. The inset shows a magnified view of the diffractograms below $2\theta = 10°$. The grey line is the expected pattern for **1** based on the crystal structure at 298(2) K.
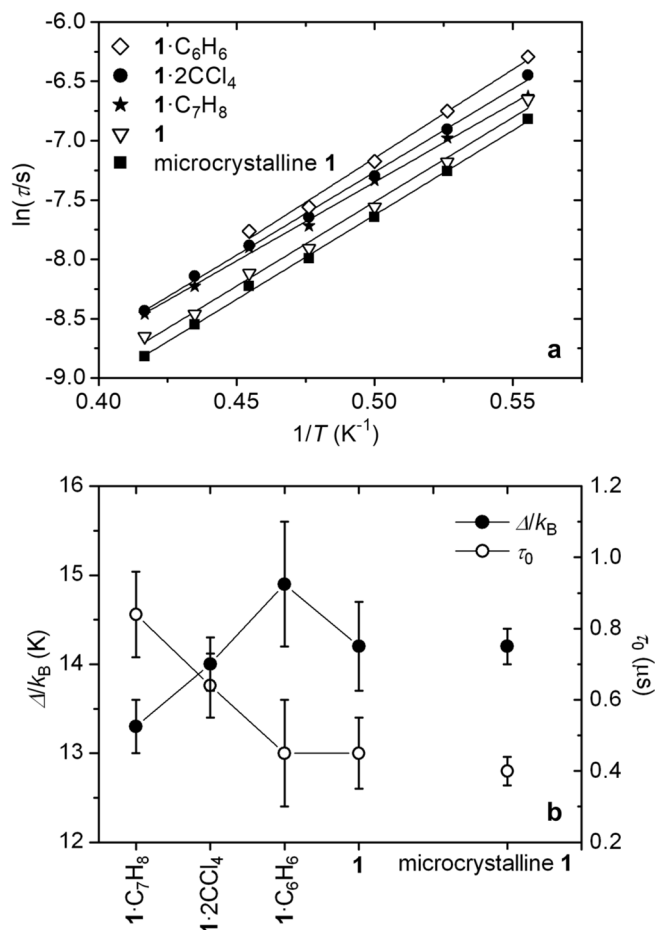

Fig. 4. Arrhenius plots of sublimed samples and of microcrystalline **1** at $H_{DC} = 1$ kOe (a), and graphical representation of the best-fit activation parameters (Δ and τ_0) so obtained (b). The vertical bars in (b) represent standard errors.

material prepared from $1·C_7H_8$, $1·2CCl_4$, and $1·C_6H_6$ behaves similarly (Fig. S1 and S2). Extraction of the relaxation times through an extended Debye model allowed to prepare the Arrhenius plots reported in Fig. 4a. The linear fitting of the different thermal relaxation profiles yielded the parameters gathered in Fig. 4b and Table S3, which immediately highlight a strict resemblance of relaxation behavior between the different samples. Irrespective of the particular compound used, the deposits have τ_0 and Δ values comparable to microcrystalline **1**. Upon closer inspection of Fig. 4b, it can be seen that the activation parameters of sublimed **1** and $1·C_6H_6$ are within experimental error from those of microcrystalline **1**. Sublimed $1·2CCl_4$ has a slightly larger τ_0, whereas the deposit prepared from $1·C_7H_8$ has a significantly larger τ_0 and a reduced Δ, suggesting more efficient through-barrier relaxation.

Fig. S3 and S4 show the temperature dependence of the width parameter α and of the $(\chi_T - \chi_S)/\chi_T$ ratio, respectively. The latter allows to evaluate the molar fraction of slowly relaxing species. The results confirm a substantially uniform magnetic dynamics throughout the series and a modest dependence of the AC properties of sublimed samples on the used pristine material. In particular, at 1.8 K the values of α and $(\chi_T - \chi_S)/\chi_T$ span a remarkably limited range in all samples, including microcrystalline **1** (0.17–0.21 and 0.87–0.92, respectively). Differences between samples are enhanced upon heating to 2.4 K, with an overall tendency of α in sublimed samples to decrease more than in microcrystalline **1**. No clear correlation appears between α and the crystallinity of the films (Fig. 3). This is reasonable, since crystallinity reflects long-range ordering while the distribution width of relaxation times is primarily sensitive to the inhomogeneity of local molecular environments.

Our findings confirm the robustness of the tetrairon(III) core, which is able to sustain the high temperature and long heating times required by the sublimation protocol with only modest effects on magnetization dynamics.

4. Conclusions

The series of known solvatomorphs of tetrairon(III) SMM $[Fe_4(L^{Ph})_2(dpm)_6]$ (**1**), namely $1·Et_2O$ [26] and $1·C_6H_6$ [34], was extended with the isolation of $1·C_7H_8$ and $1·2CCl_4$. In addition, a solvent-free phase **1** was prepared by crystallization from pentachloroethane, a bulky solvent. The X-ray structures indicate that the most important structural parameter in these propeller-like species, namely the helical pitch, is distinctly different in solvatomorphs and in unsolvated **1**. Thus, intermolecular interactions and crystal packing effects are crucial factors in determining molecular geometry. All compounds can be thermally sublimed in HV to give deposits displaying a variable degree of crystallinity. Most important, all sublimed samples show AC magnetic properties comparable to those of microcrystalline **1** in terms of activation parameters, fraction of slowly relaxing species, and width of the distribution of relaxation times, irrespective of the pristine compound used. We conclude that molecular structure has the greatest impact on the vapor-phase processability of this class of materials.

CRediT authorship contribution statement

Andrea Cornia: Conceptualization, Data curation, Formal analysis, Investigation, Methodology, Project administration, Resources, Supervision, Validation, Visualization, Writing - original draft, Writing - review & editing; **Andrea Nava:** Investigation; **Valeria Lanzilotto:** Data curation, Investigation, Methodology, Writing - review & editing; **Giordano Poneti:** Formal analysis, Funding acquisition, Investigation, Methodology, Software, Visualization, Writing - review & editing; **Matteo Mannini:** Supervision, Methodology, Validation, Writing - review & editing; **Roberta Sessoli:** Conceptualization, Methodology, Project administration, Resources, Supervision, Validation, Writing - review & editing.

Declaration of Competing Interest

The authors declare that they have no known competing financial interests or personal relationships that could have appeared to influence the work reported in this paper.

Acknowledgements

References

[1] R.J. Holmberg, M. Murugesu, Adhering magnetic molecules to surfaces, J. Mater. Chem. C 3 (46) (2015) 11986–11998, https://doi.org/10.1039/C5TC03225C.

[2] A. Cornia, D.R. Talham, M. Affronte, Thin Layers of Molecular Magnets, in: B. Sieklucka, D. Pinkowicz (Eds.), Molecular Magnetic Materials: Concepts and Applications, Wiley-VCH, Weinheim, Germany, 2017, pp. 187–229, https://doi.org/10.1002/9783527694228.

[3] A. Forment-Aliaga, E. Coronado, Hybrid Interfaces in Molecular Spintronics, Chem. Rec. 18 (7–8) (2018) 737–748, https://doi.org/10.1002/tcr.201700109.

[4] F. Ara, H. Oka, Y. Sainoo, K. Katoh, M. Yamashita, T. Komeda, Spin properties of single-molecule magnet of double-decker Tb(III)-phthalocyanine (TbPc₂) on ferromagnetic Co film characterized by spin polarized STM (SP-STM), J. Appl. Phys. 125 (2019), 183901, https://doi.org/10.1063/1.5079964.

[5] F.-S. Guo, B.M. Day, Y.-C. Chen, M.-L. Tong, A. Mansikkamäki, R.A. Layfield, Magnetic hysteresis up to 80 kelvin in a dysprosium metallocene single-molecule magnet, Science 362 (2018) 1400–1403, https://doi.org/10.1126/science.aav0652.

[6] C.A.P. Goodwin, F. Ortu, D. Reta, N.F. Chilton, D.P. Mills, Molecular magnetic hysteresis at 60 kelvin in dysprosocenium, Nature 548 (7668) (2017) 439–442, https://doi.org/10.1038/nature23447.

[7] F.-S. Guo, B.M. Day, Y.-C. Chen, M.-L. Tong, A. Mansikkamäki, R.A. Layfield, A Dysprosium Metallocene Single-Molecule Magnet Functioning at the Axial Limit, Angew. Chem. Int. Ed. 56 (38) (2017) 11445–11449, https://doi.org/10.1002/anie.201705426.

[8] R. Sessoli, Magnetic molecules back in the race, Nature 548 (7668) (2017) 400–401, https://doi.org/10.1038/548400a.

[9] T. Komeda, K. Katoh, M. Yamashita, Double-decker phthalocyanine complex: scanning tunneling microscopy study of film formation and spin properties, Prog. Surf. Sci. 89 (2014) 127–160, https://doi.org/10.1016/j.progsurf.2014.03.001.

[10] Y. Zhang, P. Liao, J. Kan, C. Yin, N. Li, J. Liu, Q. Chen, Y. Wang, W. Chen, G.Q. Xu, J. Jiang, R. Berndt, K. Wu, Low-temperature scanning tunneling microscopy study on the electronic properties of a double-decker DyPc₂ molecule at the surface, Phys. Chem. Chem. Phys. 17 (40) (2015) 27019–27026, https://doi.org/10.1039/C5CP03925H.

[11] A. Lodi Rizzini, C. Krull, A. Mugarza, T. Balashov, C. Nistor, R. Piquerel, S. Klyatskaya, M. Ruben, P.M. Sheverdyaeva, P. Moras, C. Carbone, C. Stamm, P. S. Miedema, P.K. Thakur, V. Sessi, M. Soares, F. Yakhou-Harris, J.C. Cezar, S. Stepanow, P. Gambardella, Coupling of single, double, and triple-decker metal-phthalocyanine complexes to ferromagnetic and antiferromagnetic substrates, Surf. Sci. 630 (2014) 361–374, https://doi.org/10.1016/j.susc.2014.07.008.

[12] L. Malavolti, L. Poggini, L. Margheriti, D. Chiappe, P. Graziosi, B. Cortigiani, V. Lanzilotto, F. Buatier de Mongeot, P. Ohresser, E. Otero, F. Choueikani, P. Sainctavit, I. Bergenti, V.A. Dediu, M. Mannini, R. Sessoli, Magnetism of TbPc₂ SMMs on ferromagnetic electrodes used in organic spintronics, Chem. Commun. 49 (2013) 11506–11508, https://doi.org/10.1039/c3cc46868b.

[13] D. Klar, A. Candini, L. Joly, S. Klyatskaya, B. Krumme, P. Ohresser, J.-P. Kappler, M. Ruben, H. Wende, Hysteretic behaviour in a vacuum deposited submonolayer of single ion magnets, Dalton Trans. 43 (28) (2014) 10686–10689, https://doi.org/10.1039/C4DT01005A.

[14] L. Margheriti, D. Chiappe, M. Mannini, P.-E. Car, P. Sainctavit, M.-A. Arrio, F. Buatier de Mongeot, J.C. Cezar, F.M. Piras, A. Magnani, E. Otero, A. Caneschi, R. Sessoli, X-ray detected magnetic hysteresis of thermally evaporated terbium double-decker oriented films, Adv. Mater. 22 (48) (2010) 5488–5493, https://doi.org/10.1002/adma.201003275.

[15] J. Dreiser, C. Wäckerlin, M.E. Ali, C. Piamonteze, F. Donati, A. Singha, K. S. Pedersen, S. Rusponi, J. Bendix, P.M. Oppeneer, T.A. Jung, H. Brune, Exchange interaction of strongly anisotropic tripodal erbium single-ion magnets with

[16] metallic surfaces, ACS Nano 8 (5) (2014) 4662–4671, https://doi.org/10.1021/nn500409u.

[16] J. Dreiser, G.E. Pacchioni, F. Donati, L. Gragnaniello, A. Cavallin, K.S. Pedersen, J. Bendix, B. Delley, M. Pivetta, S. Rusponi, H. Brune, Out-of-Plane Alignment of Er (trensal) Easy Magnetization Axes Using Graphene, ACS Nano 10 (2) (2016) 2887–2892, https://doi.org/10.1021/acsnano.5b08178.

[17] J. Dreiser, C. Wäckerlin, M. Buzzi, K.S. Pedersen, J. Bendix, Island formation of Er (trensal) single-ion magnets on graphene observed on the micrometer scale, RSC Adv. 11 (16) (2021) 9421–9425, https://doi.org/10.1039/D1RA00783A.

[18] S.G. Miralles, A. Bedoya-Pinto, J.J. Baldoví, W. Cañon-Mancisidor, Y. Prado, H. Prima-Garcia, A. Gaita-Ariño, G. Mínguez Espallargas, L.E. Hueso, E. Coronado, Sublimable chloroquinolinate lanthanoid single-ion magnets deposited on ferromagnetic electrodes, Chem. Sci. 9 (1) (2018) 199–208, https://doi.org/10.1039/C7SC03463F.

[19] C. Gao, Q. Yang, B.-W. Wang, Z.-M. Wang, S. Gao, Evaporable lanthanide single-ion magnet, CrystEngComm 18 (22) (2016) 4165–4171, https://doi.org/10.1039/C5CE02571K.

[20] Y. Bi, C. Chen, Y.-F. Zhao, Y.-Q. Zhang, S.-D. Jiang, B.-W. Wang, J.-B. Han, J.-L. Sun, Z.-Q. Bian, Z.-M. Wang, S. Gao, Thermostability and photoluminescence of Dy(III) single-molecule magnets under a magnetic field, Chem. Sci. 7 (2016) 5020–5031, https://doi.org/10.1039/C6SC01157H.

[21] K. Katoh, H. Isshiki, T. Komeda, M. Yamashita, Multiple-decker phthalocyaninato Tb(III) single-molecule magnets and Y(III) complexes for next generation devices, Coord. Chem. Rev. 255 (17-18) (2011) 2124–2148, https://doi.org/10.1016/j.ccr.2011.02.024.

[22] X. Yi, K. Bernot, F. Pointillart, G. Poneti, G. Calvez, C. Daiguebonne, O. Guillou, R. Sessoli, A luminescent and sublimable Dyᴵᴵᴵ-based single-molecule magnet, Chem. - Eur. J. 18 (36) (2012) 11379–11387, https://doi.org/10.1002/chem.201201167.

[23] E. Kiefl, M. Mannini, K. Bernot, X. Yi, A. Amato, T. Leviant, A. Magnani, T. Prokscha, A. Suter, R. Sessoli, Z. Salman, Robust Magnetic Properties of a Sublimable Single-Molecule Magnet, ACS Nano 10 (6) (2016) 5663–5669, https://doi.org/10.1021/acsnano.6b01817.

[24] D.S. Krylov, S. Schimmel, V. Dubrovin, F. Liu, T.T.N. Nguyen, L. Spree, C.-H. Chen, G. Velkos, C. Bulbucan, R. Westerström, M. Studniarek, J. Dreiser, C. Hess, B. Büchner, S.M. Avdoshenko, A.A. Popov, Substrate-Independent Magnetic Bistability in Monolayers of the Single-Molecule Magnet Dy₂ScN@C₈₀ on Metals and Insulators, Angew. Chem. Int. Ed. 59 (14) (2020) 5756–5764, https://doi.org/10.1002/anie.201913955.

[25] A. Cornia, M. Mannini, R. Sessoli, D. Gatteschi, Propeller-Shaped Fe₄ and Fe₃M Molecular Nanomagnets: A Journey from Crystals to Addressable Single Molecules, Eur. J. Inorg. Chem. 2019 (2019) 552–568, https://doi.org/10.1002/ejic.201801266.

[26] S. Accorsi, A.-L. Barra, A. Caneschi, G. Chastanet, A. Cornia, A.C. Fabretti, D. Gatteschi, C. Mortalò, E. Olivieri, F. Parenti, P. Rosa, R. Sessoli, L. Sorace, W. Wernsdorfer, L. Zobbi, Tuning anisotropy barriers in a family of tetrairon(III) single-molecule magnets with an S = 5 ground state, J. Am. Chem. Soc. 128 (14) (2006) 4742–4755, https://doi.org/10.1021/ja0576381.

[27] L. Margheriti, M. Mannini, L. Sorace, L. Gorini, D. Gatteschi, A. Caneschi, D. Chiappe, R. Moroni, F. Buatier de Mongeot, A. Cornia, F.M. Piras, A. Magnani, R. Sessoli, Thermal deposition of intact tetrairon(III) single-molecule magnets in high-vacuum conditions, Small 5 (12) (2009) 1460–1466, https://doi.org/10.1002/smll.200801594.

[28] L. Malavolti, V. Lanzilotto, S. Ninova, L. Poggini, I. Cimatti, B. Cortigiani, L. Margheriti, D. Chiappe, E. Otero, P. Sainctavit, F. Totti, A. Cornia, M. Mannini, R. Sessoli, Magnetic bistability in a submonolayer of sublimated Fe₄ single-molecule magnets, Nano Lett. 15 (1) (2015) 535–541, https://doi.org/10.1021/nl503925h.

[29] V. Lanzilotto, L. Malavolti, S. Ninova, I. Cimatti, L. Poggini, B. Cortigiani, M. Mannini, F. Totti, A. Cornia, R. Sessoli, The Challenge of Thermal Deposition of Coordination Compounds: Insight into the Case of an Fe₄ Single Molecule Magnet, Chem. Mater. 28 (2016) 7693–7702, https://doi.org/10.1021/acs.chemmater.6b02696.

[30] J.A.J. Burgess, L. Malavolti, V. Lanzilotto, M. Mannini, S. Yan, S. Ninova, F. Totti, S. Rolf-Pissarczyk, A. Cornia, R. Sessoli, S. Loth, Magnetic fingerprint of individual Fe₄ molecular magnets under compression by a scanning tunnelling microscope, Nat. Commun. 6 (2015) 8216, https://doi.org/10.1038/ncomms9216.

[31] L. Rigamonti, M. Piccioli, L. Malavolti, L. Poggini, M. Mannini, F. Totti, B. Cortigiani, A. Magnani, R. Sessoli, A. Cornia, Enhanced vapor-phase processing in fluorinated Fe₄ single-molecule magnets, Inorg. Chem. 52 (10) (2013) 5897–5905, https://doi.org/10.1021/ic400037c.

[32] S. Ninova, V. Lanzilotto, L. Malavolti, L. Rigamonti, B. Cortigiani, M. Mannini, F. Totti, R. Sessoli, Valence electronic structure of sublimated Fe₄ single-molecule magnets: an experimental and theoretical characterization, J. Mater. Chem. C 2 (2014) 9599–9608, https://doi.org/10.1039/C4TC01647E.

[33] G. Serrano, L. Poggini, M. Briganti, A.L. Sorrentino, G. Cucinotta, L. Malavolti, B. Cortigiani, E. Otero, P. Sainctavit, S. Loth, F. Parenti, A.-L. Barra, A. Vindigni, A. Cornia, F. Totti, M. Mannini, R. Sessoli, Quantum dynamics of a single molecule magnet on superconducting Pb(111), Nat. Mater. 19 (5) (2020) 546–551, https://doi.org/10.1038/s41563-020-0608-9.

[34] L. Vergnani, A.L. Barra, P. Neugebauer, M.J. Rodriguez-Douton, R. Sessoli, L. Sorace, W. Wernsdorfer, A. Cornia, Magnetic Bistability of Isolated Giant-Spin Centers in a Diamagnetic Crystalline Matrix, Chem. - Eur. J. 18 (11) (2012) 3390–3398, https://doi.org/10.1002/chem.201103251.

[35] W.L.F. Armarego, C.L.L. Chai, Purification of laboratory chemicals, 5th ed., Butterworth-Heinemann, Burlington, United States, 2003.

[36] A.I. Vogel, Vogel's Textbook of Practical Organic Chemistry, 5th ed., revised by B. S. Furniss, A.J. Hannaford, P.W.G. Smith, A.R. Tatchell, Longman Scientific & Technical, Harlow, United Kingdom, 1989.

[37] A. Altomare, G. Cascarano, C. Giacovazzo, A. Guagliardi, M.C. Burla, G. Polidori, M. Camalli, SIR 92 – a program for automatic solution of crystal structures by direct methods, J. Appl. Crystallogr. 27 (1994) 435, https://doi.org/10.1107/S002188989400021X.

[38] G.M. Sheldrick, Crystal structure refinement with SHELXL, Acta Crystallogr., Sect. C: Struct. Chem. 71 (2015) 3–8, https://doi.org/10.1107/S2053229614024218.

[39] L.J. Farrugia, WinGX and ORTEP for Windows: an update, J. Appl. Crystallogr. 45 (4) (2012) 849–854, https://doi.org/10.1107/S0021889812029111.

[40] Persistence of Vision Pty. Ltd., Persistence of Vision Raytracer (Version 3.7) [Computer software], retrieved from http://www.povray.org/download/, 2021.

[41] C.F. Macrae, I. Sovago, S.J. Cottrell, P.T.A. Galek, P. McCabe, E. Pidcock, M. Platings, G.P. Shields, J.S. Stevens, M. Towler, P.A. Wood, Mercury 4.0: from visualization to analysis, design and prediction, J. Appl. Crystallogr. 53 (2020) 226–235, https://doi.org/10.1107/S1600576719014092.

[42] C.V. Topping, S.J. Blundell, A.C. susceptibility as a probe of low-frequency magnetic dynamics, J. Phys.: Condens. Matter 31 (2019), 013001, https://doi.org/10.1088/1361-648X/aaed96.

[43] L. Gregoli, C. Danieli, A.-L. Barra, P. Neugebauer, G. Pellegrino, G. Poneti, R. Sessoli, A. Cornia, Magnetostructural correlations in tetrairon(III) single-molecule magnets, Chem. - Eur. J. 15 (26) (2009) 6456–6467, https://doi.org/10.1002/chem.200900483.

[44] J. Mayans, M. Font-Bardia, A. Escuer, Chiroptical and magnetic properties of star-shaped Fe^{III}_4 complexes from chiral Schiff bases. Structural and magnetic correlations based on continuous shape measures, Dalton Trans. 47 (25) (2018) 8392–8401, https://doi.org/10.1039/C8DT01684D.